GOMOS Level 2 evolution studies (ALGOM)

Aerosol-insensitive ozone retrievals in the UTLS

FMI-ALGOM-TN-TWOSTEP-201
March 2016

V.F. Sofieva. E. Kyrölä, J. Tamminen, J.Hakkarainen

Finnish Meteorological Institute, Helsinki, Finland

Contents

1 Introduction

In the previous studies performed within the WP 1 of the ALGOM project, it was shown that retrievals of ozone, aerosols and NO2 in the UTLS are very sensitive to the assumed aerosol model. By changing the aerosol model from a second-degree polynomial to a first-degree polynomial, ozone and aerosols in the UTLS may change up to a factor of two in the UTLS, and associated changed in retrieved NO2 can change up to a few hundreds of percent. The studies performed earlier with a linear aerosol extinction model used in the two-step inversion (Sofieva et al., 2015) have shown a significant improvements of ozone profiles in the UTLS (a large positive ozone bias observed in V6 data is dramatically reduced). However, such sensitivity of retrievals to the assumed aerosol model indicates large systematic uncertainty of the data retrieved with the baseline GOMOS algorithm or its analogue with another aerosol model developed previously within the ALGOM project.

The main motivation for this study is development of aerosol-insensitive ozone retrievals in the UTLS. Using triplets in the Chappuis band - the method which is often used in retrievals from limb-scattering instruments - has allowed a simple and a robust inversion in the UTLS, which only assumes that the aerosol extinction is linear in a relatively narrow wavelength band.

The Technical Note is organized as follows. In Section 2, the retrieval method is described. The extensive assessment of the retrieval results is presented in Section 3. Summary and discussion (Section 4) concludes the TN.

2 Aerosol- insensitive retrievals in the UTLS

The proposed inversion consists of the following steps:

1. Inversion using visible triplets in the UTLS;

2. Forming the resulting ozone profile using the V6 ozone profiles in the middle atmosphere and the weighted mean of V6 and the new triplet profile in the UTLS.

Below we describe each step in detail.

2.1 Triplet inversion in the UTLS

We will use the wavelengths as in the classical triplet method by [*Flittner et al.*, 2000]: the reference wavelengths near 525 and 675 nm and absorbing wavelengths near 600 nm. Since stars are relatively weak sources of light, several pixels are used for reference and absorbing wavelengths (Figure 1). Using differential optical depth allows nearly cancelling scintillation-dilution perturbations and a significant reduction of uncertainty due to Rayleigh scattering correction based on the ECMWF field. The Level 1 b transmission spectra $T_{L1b}(\lambda)$ at a given tangent altitudes can be expressed as:

$$T_{L1b}(\lambda) = T_{ext}(\lambda) \cdot T_{dil}(\lambda) \cdot T_{sc}(\lambda), \quad (1)$$

where $T_{dil}(\lambda)$ and $T_{sc}(\lambda)$ are transmittances due to dilution and scintillation, respectively.

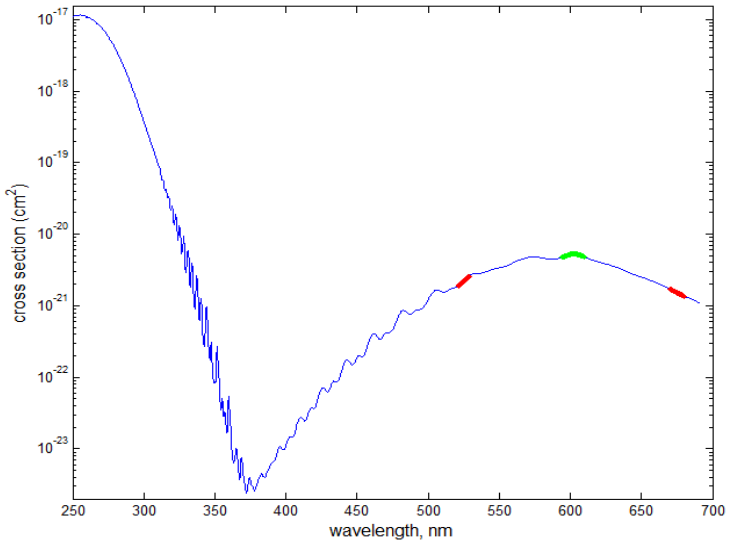

Figure 1. Reference (red, 521-529 nm and 670-680 nm) and absorbing (green, 592-612 nm) wavelengths.

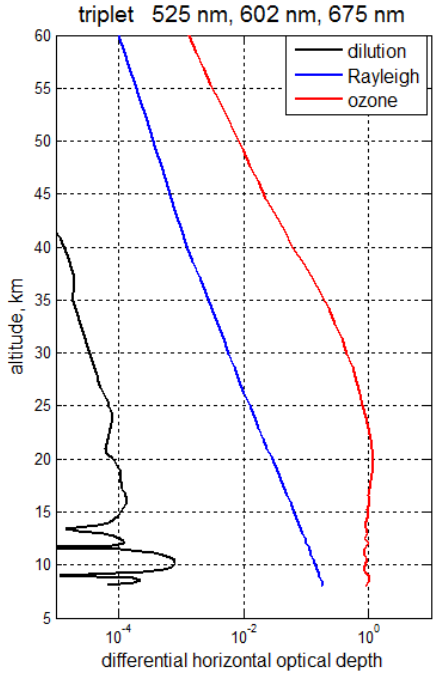

Figure 2. Differential horizontal optical depth for the visible triplet 525 nm, 602 nm, 675 nm due to ozone absorption, Rayleigh scattering and dilution. The contributions are computed based on the occultation R04078/S002.

The differential optical depth $d\tau$:

$$d\tau = \tau(\lambda_{ab}) - \tfrac{1}{2}\cdot\left(\left\langle\tau(\lambda_{r1})\right\rangle + \left\langle\tau(\lambda_{r2})\right\rangle\right)$$
$$\tau = -\log(T_{L1b}) \qquad (2)$$

where λ_{ab} is absorbing wavelength, λ_{r1} and λ_{r2} are reference wavelengths, has contributions due to ozone absorption, Rayleigh and aerosol scattering, and due to refractive effects. However, due to the selected wavelengths, ozone contribution to the differential optical depth strongly dominates. This is illustrated in Figure 2, which compares the contributions of ozone absorption, Rayleigh scattering and dilution (refractive attenuation) to the differential horizontal optical depth for the visible triplet 525 nm, 602 nm, 675 nm. This means that Level 1b transmittances, without dilution and scintillation correction, can be used for the inversion from the visible triplets. The contribution from Rayleigh scattering to the differential optical depth is significantly smaller than that of ozone, but it can be as large as a few percent in the UTLS. Therefore, the Rayleigh optical depth is estimated (using the ECMWF field) and subtracted from the total optical depth data.

Computation of optical depth (taking logarithm) requires good signal-to-noise ratio. Only the pixels with the signal-to-noise ratio larger than 3 are used in the inversion. The uncertainty of the optical depth σ_τ is approximated as

$$\sigma_\tau = \frac{\sigma_T}{T}, \tag{3}$$

where σ_T is uncertainty of transmittance *T*.

As mentioned above, Level 1 b data are used without scintillation and dilution correction. The retrievals of ozone line density from visible triplet are performed only in the UTLS, i.e., at altitudes below z_t+7 km, z_t is the tropopause height.

The average optical depth for reference channels $\langle \tau(\lambda_{r1}) \rangle$ and $\langle \tau(\lambda_{r2}) \rangle$ is used, and the triplet optical depth is computed for each channel at absorbing wavelengths 592-612 nm according to Eq.(2). The uncertainties of the differential optical depth values (Eq.(2)) are computed as:

$$\sigma_{d\tau}^2 = \sigma_\tau^2 + \frac{1}{4}\sigma_{r1}^2 + \frac{1}{4}\sigma_{r2}^2, \tag{4}$$

where σ_τ is uncertainty in the absorbing channel , σ_{r1} and σ_{r2} are uncertainties of the average optical depth in the reference channels.

Ozone line density is estimated for each pixel in absorbing channels $\mathrm{O}_3(\lambda) = d\tau(\lambda) / \mathrm{D}_{cross}(\lambda)$, where $\mathrm{D}_{cross}(\lambda)$ is the differential cross-sections corresponding to a triplet, and the weighted mean of these estimates $\bar{\mathrm{O}}_3$ is computed (with weights inversely proportional to uncertainties $\sigma_{\mathrm{O3}}^2(\lambda_i)$ for individual absorbing channels). The associated uncertainty of the triplet line density $\bar{\mathrm{O}}_3$ is estimated as:

$$\sigma_{\bar{\mathrm{O}}_3}^2 = \frac{1}{\sum_{i=1}^{N} 1/\sigma_{\mathrm{O3}}^2(\lambda_i)} \cdot \frac{1}{(N-1)} \sum_{i=1}^{N} \frac{(\mathrm{O}_3(\lambda_i) - \bar{\mathrm{O}}_3)^2}{\sigma_{\mathrm{O3}}^2(\lambda_i)} \tag{5}$$

In Eq. (5), the first factor is the uncertainty of the weighted mean provided the uncertainties $\sigma_{\mathrm{O3}}^2(\lambda_i)$ are the only source of variations in ozone. The second factor in Eq. (5) takes into account variability between the different values of $\mathrm{O}_3(\lambda_i)$.

2.2 *Combining V6 and triplet line densities*

The combining V6 and triplet ozone profiles is performed in the UTLS (from 6 km above the tropopause until the end of occultation).

The uncertainty of V6 is modified by adding a function increasing linearly from 0% at (z_t+6 km), z_t being the tropopause height, to 20% at z_t, with the saturation level of 20% below z_t (Figure 3, left). Such modification characterizes the systematic uncertainty of V6 ozone line density due to uncertainty of the aerosol model. The combined ozone profile is the weighted mean of the V6 and triplet line density profiles with the weights inversely proportional to uncertainties: modified V6 uncertainty for V6 profile and $\sigma_{\bar{O}_3}$ (Eq.(5)) for the triplet inversion (Figure 3, center). As a result, above (z_t + 6 km), ozone profile follows exactly V6 data. Below (z_t + 6 km), the profiles are closer to the triplet inversion and practically coincide with the triplet inversion at the tropopause and below (Figure 3, right).

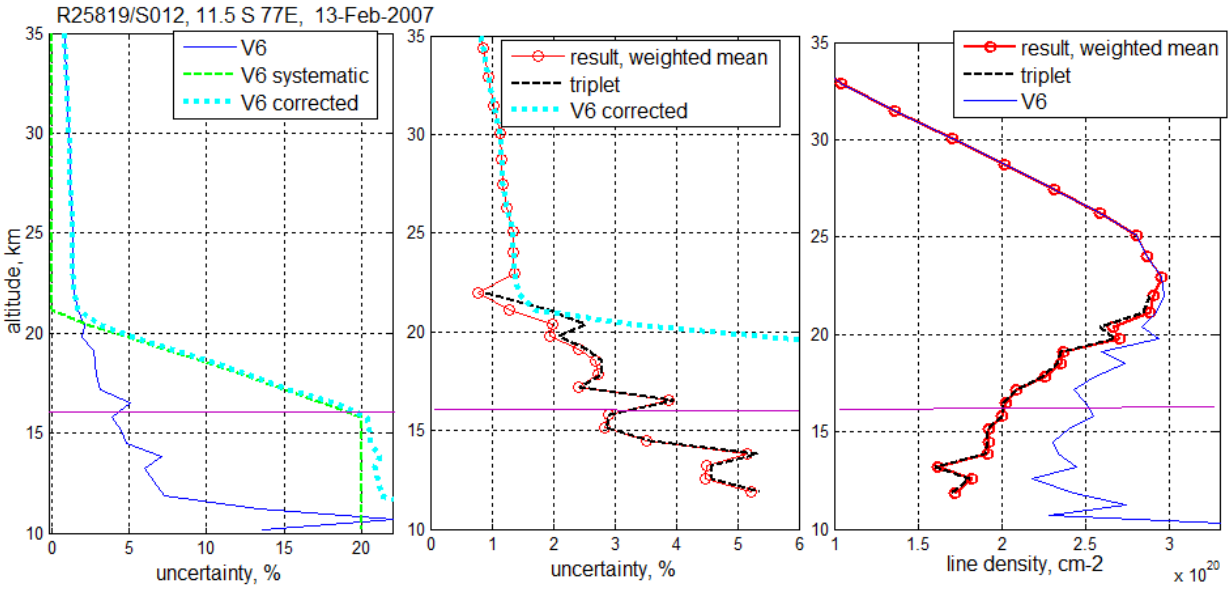

Figure 3. Illustration of combining triplet and V6 line density profiles using the data from occultation R25819/S012 (11.5°S 77°E, 13 February 2007). Left: Original uncertainty of V6 ozone line density (blue line), systematic uncertainty (green), which is added quadratically to the original V6 uncertainty, and the resulting corrected V6 uncertainty (cyan). Center: V6 corrected uncertainty (cyan, as in the left panel), the uncertainty of the triplet inversion (black) and the resulting uncertainty of the weighted mean of V6 and triplet profiles (red). Right: V6 ozone line density (blue), ozone line density from triplet inversion (black), and the weighted mean of V6 and triplet profiles (red). The lapse-rate tropopause height is ~16 km is indicated my magenta horizontal line.

If the lowest GOMOS altitude is above the tropopause, the triplet inversion is not performed and the profiles follow V6 data. After combining the ozone line density profiles, the vertical inversion is performed in the same way as for V6.

3 Assessment of the algorithm and retrieval results

All the illustrations shown in the section are based on GOMOS dark-limb occultations (with solar zenith angle at tangent point larger than 107°), which were processed with the new aerosol-insensitive algorithm.

3.1 Example of individual retrievals

To highlight the changes in retrieval results compared to version V6, the retrieved profiles for two occultations R09303/S002 and R04078/S002 are shown in Figure 4. For comparison, collocated ozonesonde profiles are also shown in Figure 4, as well as the ozone profiles retrieved with the previous processing version ("GOMLAB", linear in $1/\lambda$ aerosol model) (Sofieva et al., 2016). As observed in Figure 4, the retrieved ozone profiles with the aerosol-insensitive method are much closer to the ozonesonde profiles than V6, and they are not worse in the UTLS than the profiles retrieved assuming the linear aerosol model.

It is worth to note that the results of the new retrievals are very stable with respect to some variations in reference and absorbing wavelength used in the triplet inversion.

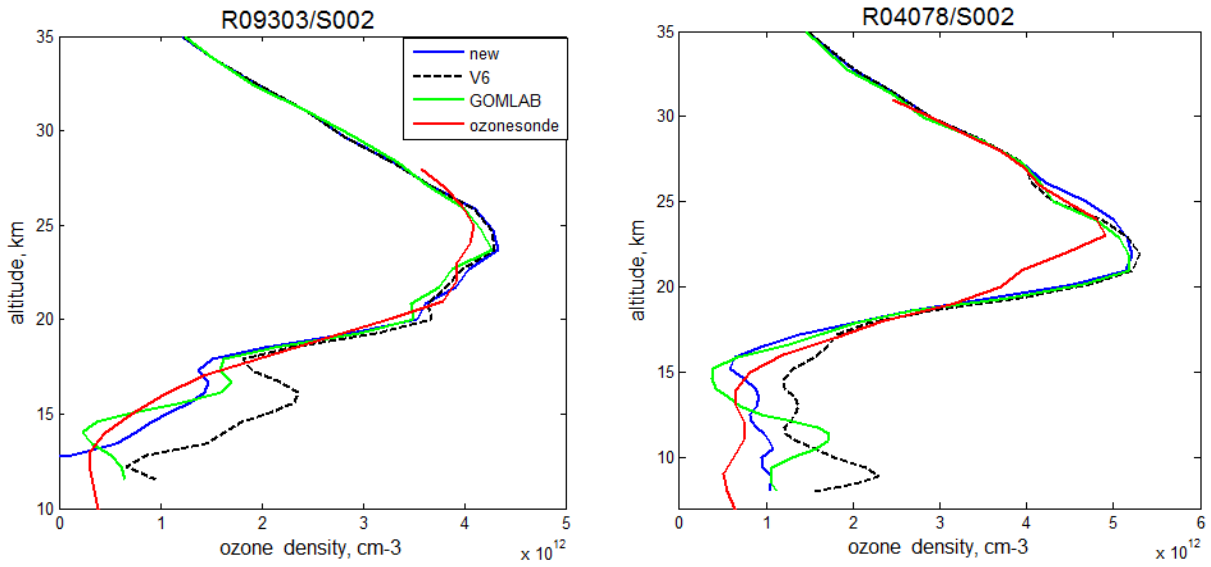

Figure 4. Ozone profiles for occultations R09303/S002 (left) and R04078/S002(right) for the aerosol-insensitive retrievals ("new") compared to V6, ozone sonde at Izana, and the previous version of the processor ("GOMLAB").

3.2 Validation against NDACC ozonesondes

For validation against the NDACC ozonesondes, we have used the same data as in validation of V6 dataset in WP1.1. The selected data are separated less than 1000 km in ground distance, less than 3° in latitude and less than 24 hours in time. The information about the location of ozonesonde stations having a significant number of collocated profiles below the tropopause is collected in Table 1. In the following, we show the results of comparisons for 50 brightest stars in GOMOS catalogue (star_id <50); occultation of dim stars do not go usually below the tropopause.

Table 1. Number of collocated GOMOS and ozonesonde profiles in UTLS and troposphere for the NDACC stations included in the comparison.

Station (Lat °N, Lon °E)	**Number of collocations in UTLS**	**Number of collocations in troposphere**
Izaña (28.30, -16.50)	103	42
Neumayer (-70.68, -8.26)	60	6
Ny Alesund (78.93, 11.93)	110	14
Paramaribo (5.8, -55.22)	50	3
Reunion (-21.06, 55.48)	54	20

Figures 8-12 show the results of the validation of new GOMOS ozone profiles (labeled as "new") against NDACC ozonesondes. For comparison, the results for V6 ozone profiles are also shown. For tropical stations, the dramatic reduction of biases is observed. The new profiles are nearly unbiased with respect to ozonesonde data. At polar stations, the GOMLAB results are not worse than those of V6 (at polar stations, also V6 data have a small bias in the UTLS in comparisons with ozonesondes). Also reduction of the spread in the UTLS is clearly observed for new retrievals.

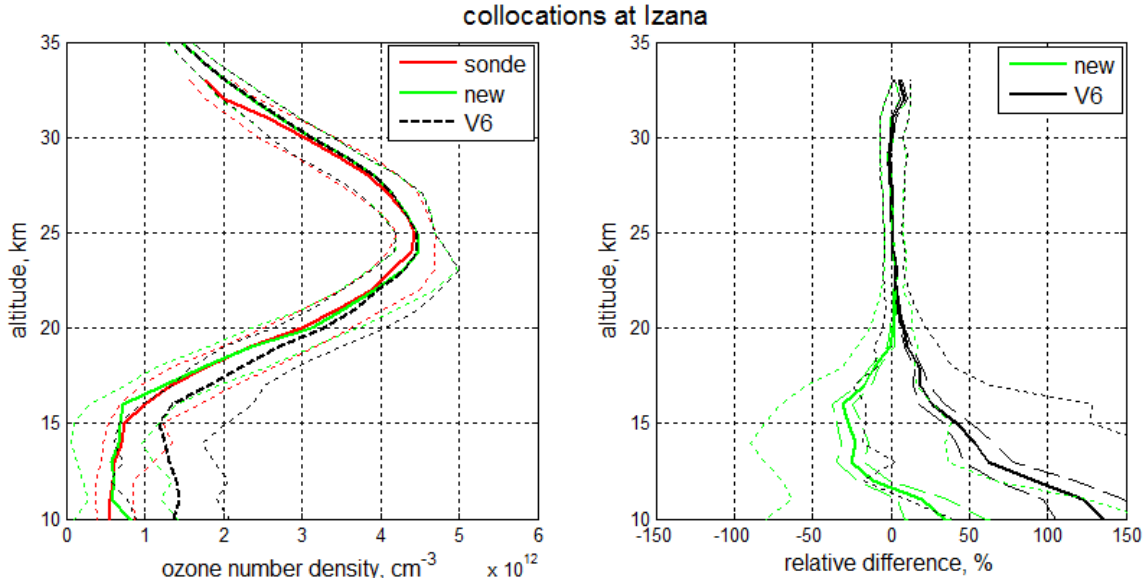

Figure 5. Statistics of comparison with ozonesondes at Izana. Left: median profiles (solid lines) and 16th and 84th percentiles (dotted lines). Right: solid lines: median of relative differences, dotted lines: 16th and 84th percentiles, dashed lines: the standard error of the mean.

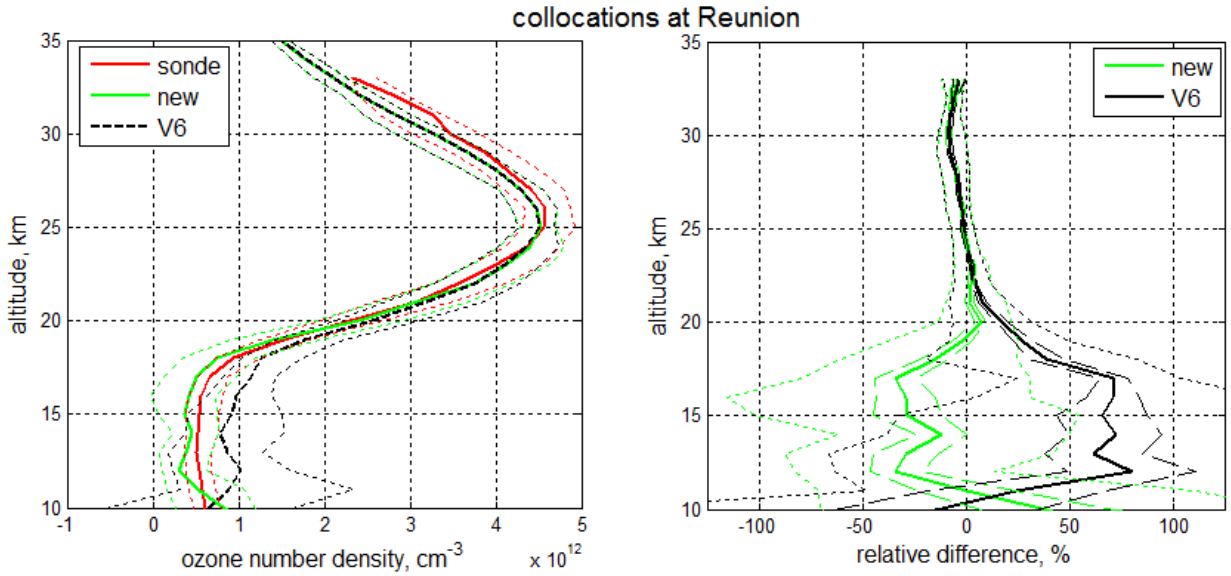

Figure 6. As Figure 5, but for collocations at Reunion.

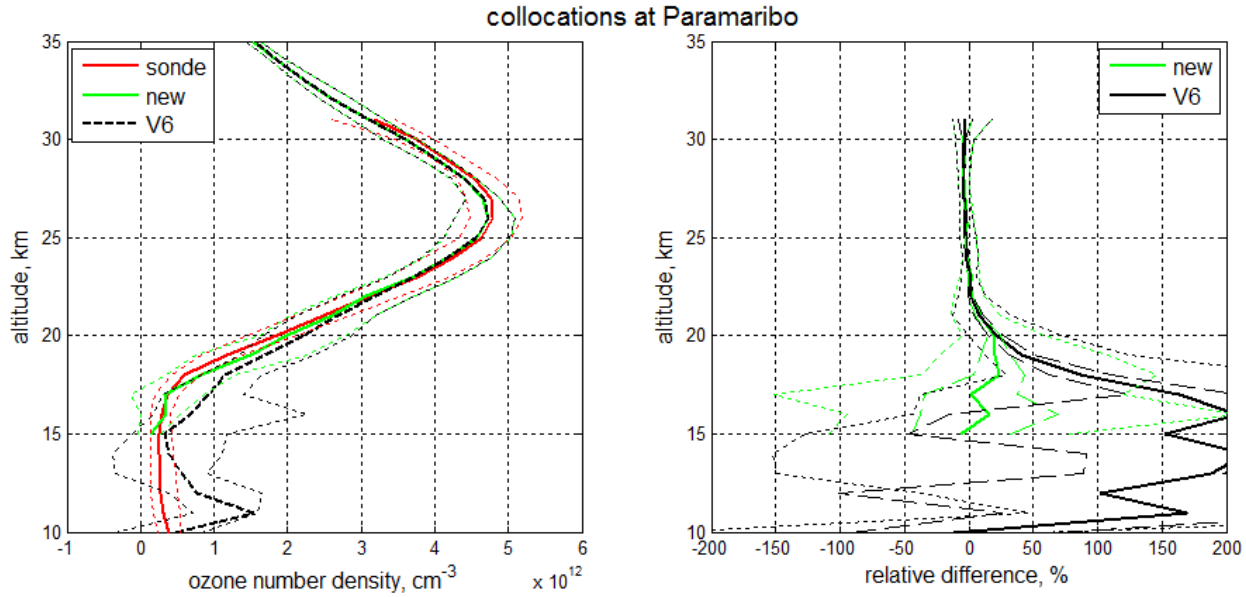

Figure 7. As Figure 5, but for collocations at Paramaribo.

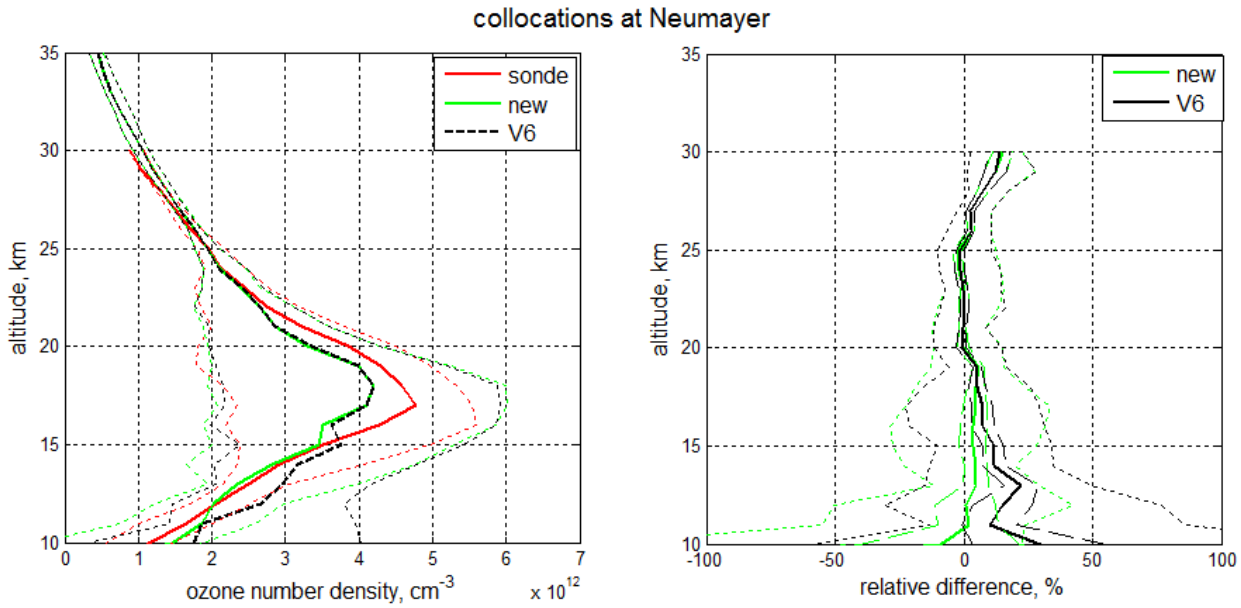

Figure 8. As Figure 5, but for collocations at Neumayer.

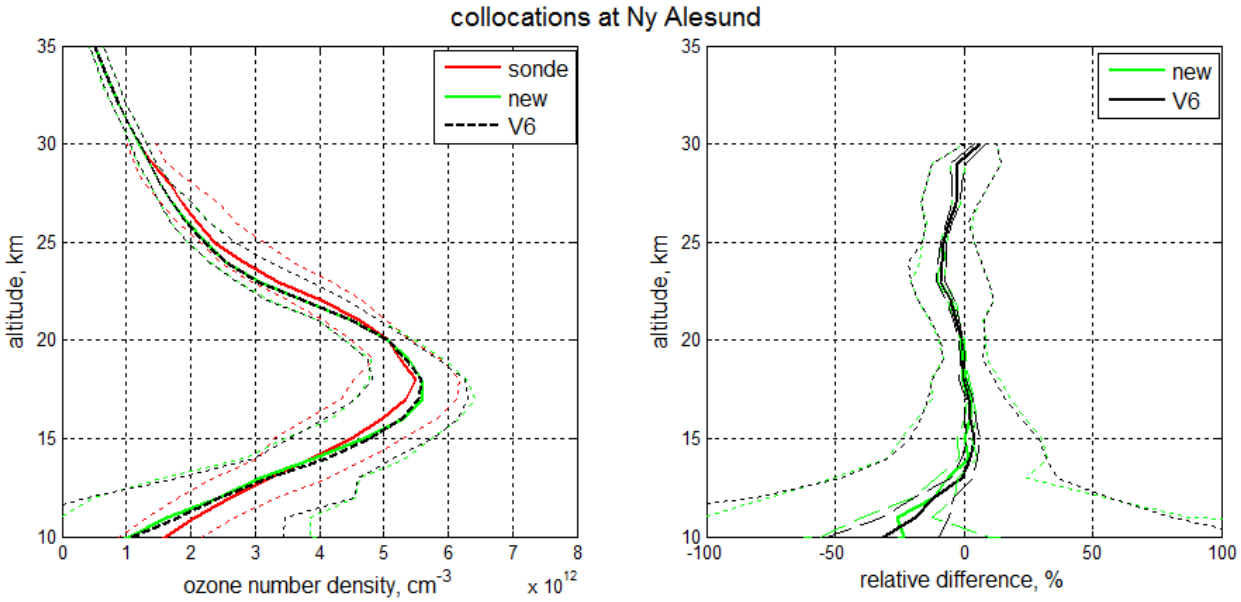

Figure 9. As Figure 5, but for collocations at Ny Alesund.

3.3 Geophysical illustrations using new GOMOS ozone data: focus on the UTLS

For illustrations used in this section, the whole GOMOS dataset of dark-limb occultations is processed. The collection of ozone data is the same as used in the Ozone_cci HARMOZ dataset [*Sofieva et al.*, 2013]. Additionally, occultations of "bad stars" according to the new list (Kyrölä et al., 2017, FMI-ALGOM-TN-005) are removed. After the processing, the ozone data were screened for outliers according to recommendations written in GOMOS IPF 6.0 Disclaimer.

As an illustration of a larger dataset, the GOMOS ozone profiles in the equatorial region (latitudes 20°S-20°N) in 2007-2008 are compared with ozone profiles from other satellite instruments (MIPAS, OSIRIS and ACE-FTS), which have been already used in several scientific studies in the UTLS. As observed in Figure 10 (left), the V6 ozone profiles are strongly biased in the tropical UTLS, while new data are close to the profiles by other satellite instruments. The mean uncertainty of new GOMOS data is larger in the UTLS than that of V6 data, but not dramatically.

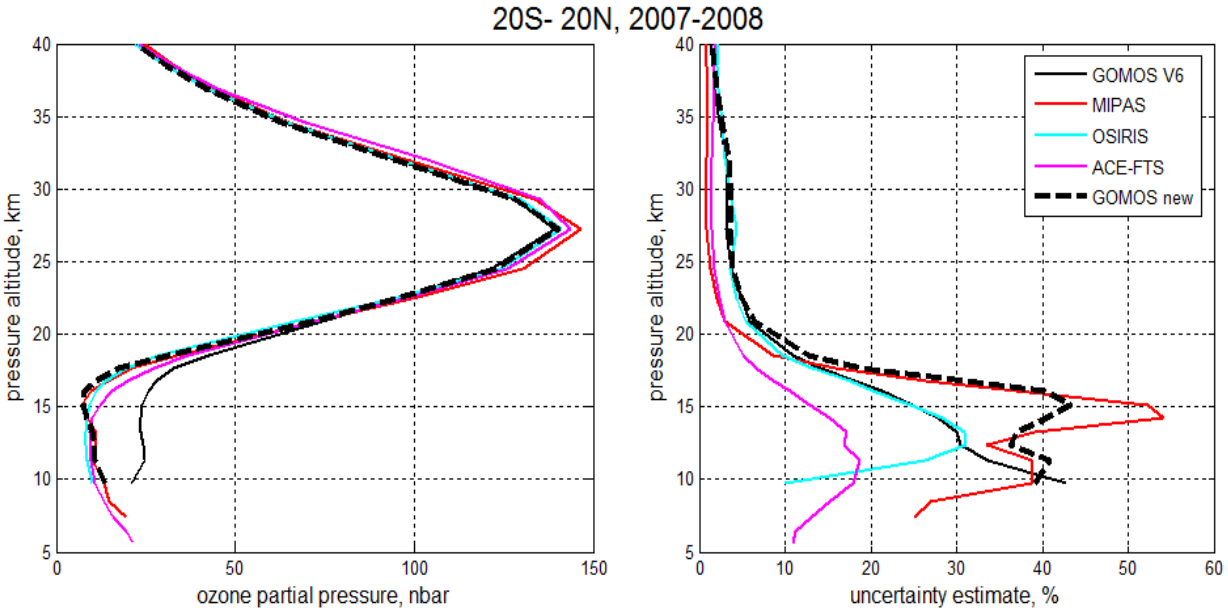

Figure 10. Left: mean ozone profiles at 20°S-20°N in 2007-2008 for GOMOS V6, MIPAS, OSIRIS, ACE-FTS and the aerosol-insensitive GOMOS processor ('GOMOS new'). Right: mean ozone uncertainty estimates for each instrument.

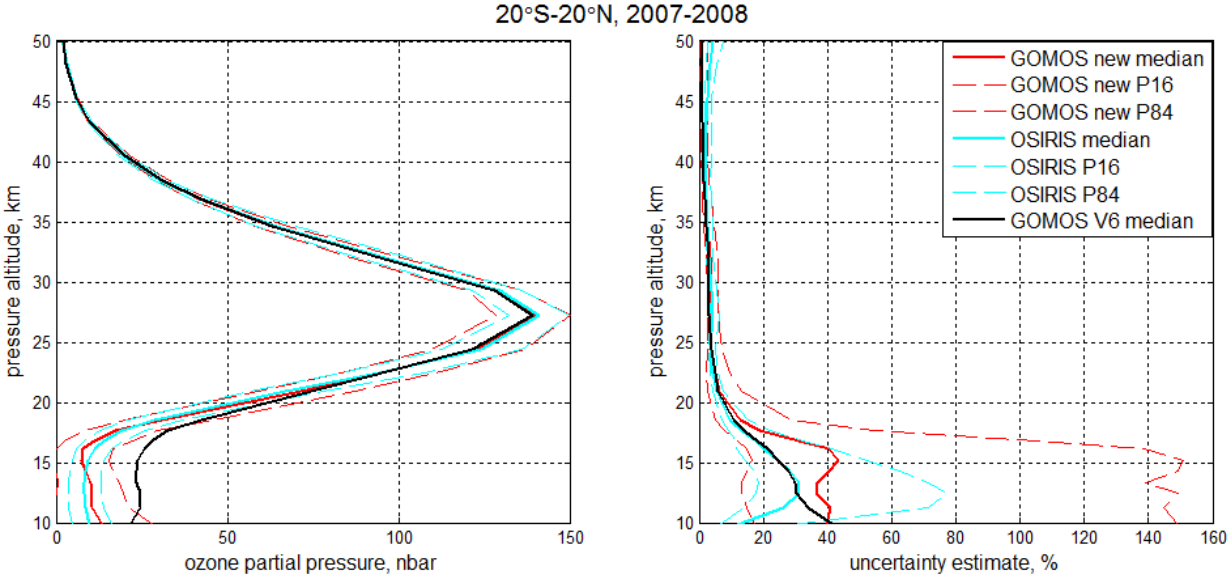

Figure 11. Left: mean ozone profiles at 20°S-20°N in 2007-2008 for GOMOS V6, OSIRIS and the aerosol-insensitive GOMOS processor (solid lines) and variability characterized by 16th and 84th percentiles of the distributions (dashed lines). Right: median uncertainty estimates and percentiles on the uncertainty distributions. In both panels, only median profiles are shown for GOMOS V6 ozone data.

A more detailed comparison of new and V6 GOMOS ozone profiles with OSIRIS data in the equatorial region for the same period 2007-2008 is shown in Figure 11. A very good agreement of GOMOS and OSIRIS profiles in the middle stratosphere can be noticed on the left panel of Figure 11. For the aerosol-insensitive retrievals presented in the TN, the mean profile is close to that of OSIRIS also in the UTLS. The variability of ozone in the UTLS is smaller in OSIRIS data compared to that of GOMOS. On the right panel, the median uncertainty estimates as well as their range characterized by 16th and 84th percentiles of the distribution are shown. The median GOMOS uncertainty in the UTLS is ~40% but overall range is large, from ~20% up to 150%. This reflects reasonably the larger variability of GOMOS ozone profiles in the UTLS.

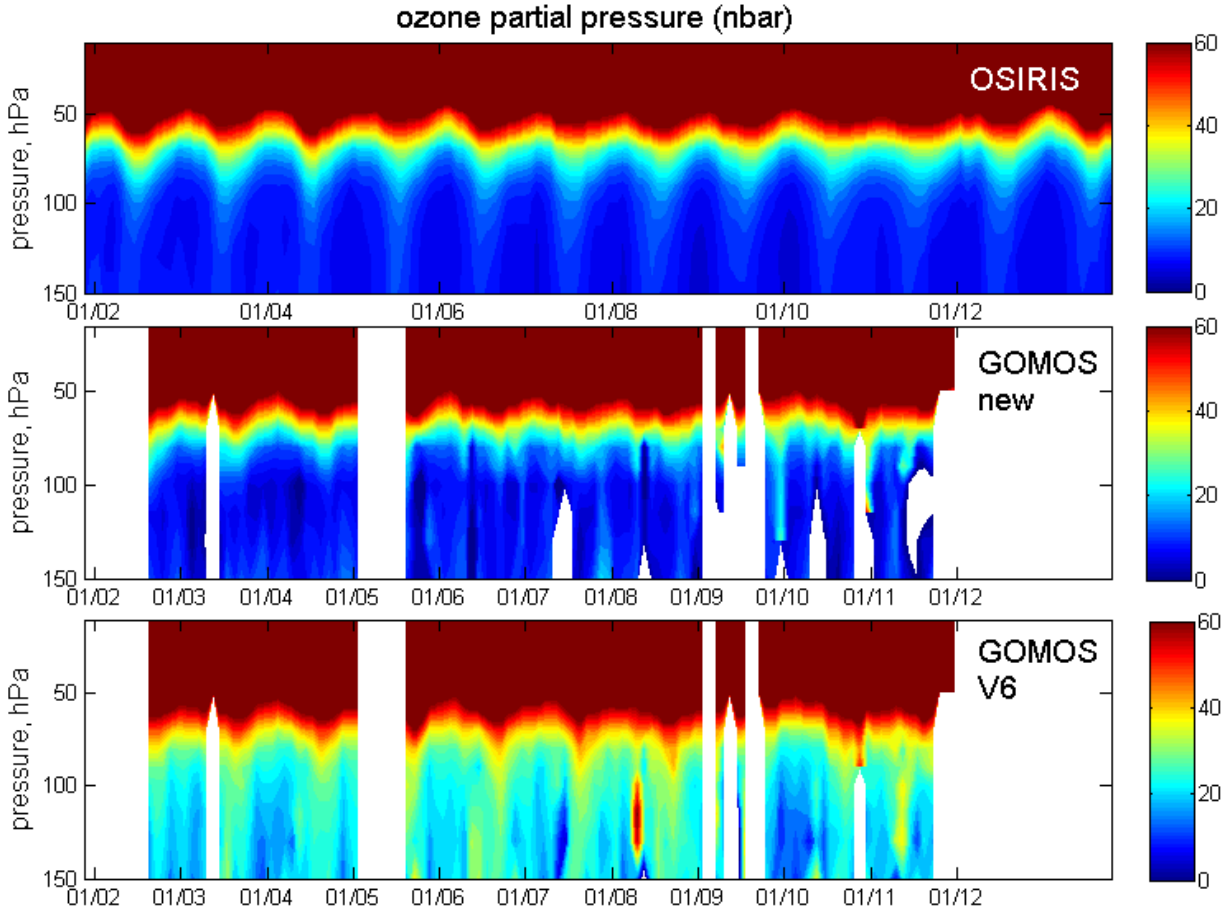

Figure 12. Time series of ozone partial pressure profiles in nbar at 20°S–20°N from OSIRIS (top), GOMOS aerosol-insensitive retrievals (center) and GOMOS V6 (bottom).

Seasonal variations and temporal evolution of ozone profiles in the UTLS is the subject of intensive research. Figure 12 shows the temporal evolution of ozone profiles in the equatorial region (20°S-20°N) from OSIRIS and two versions of GOMOS data. The pronounced seasonal cycle associated with the variations in the tropopause height are clearly observed in all datasets. The ozone values in the troposphere for the aerosol-insensitive retrievals are closer to those of OSIRIS, compared to V6 profiles. It should be noted, that the coverage of the UTLS region by GOMOS data is limited due

to applied screening (signal-to-noise ratio and “bad” stars), thus the seasonal cycle is reproduced in GOMOS data with a significant sampling uncertainty.

The Asian Summer Monsoon (ASM) contains a strong anti-cyclonic vortex in the UTLS, spanning from Asia to the Middle East. The ASM has been recognized as a significant transport pathway for water vapor and pollutants to the stratosphere (e.g., [*Park et al.*, 2007; *Kunze et al.*, 2010]). Figure 13 shows ozone distributions at 100 hPa in June-August from OSIRIS, ACE-FTS, MIPAS, SCIAMACHY and GOMOS measurements. To obtain these maps, all available data have been used. For GOMOS, the results are maps are shown for both V6 and aerosol-insensitive retrievals. The low ozone values in Asia associated with the strong upward motion of tropospheric air are clearly seen in these distributions, and peculiar features of ozone associated with the ASM are very similar in all datasets displayed. For V6, the ozone UTLS data have a significant positive offset, but lower values associated with ASM are observed in V6 distribution as well. For new GOMOS retrievals, the distribution is very similar to that by other satellite instruments.

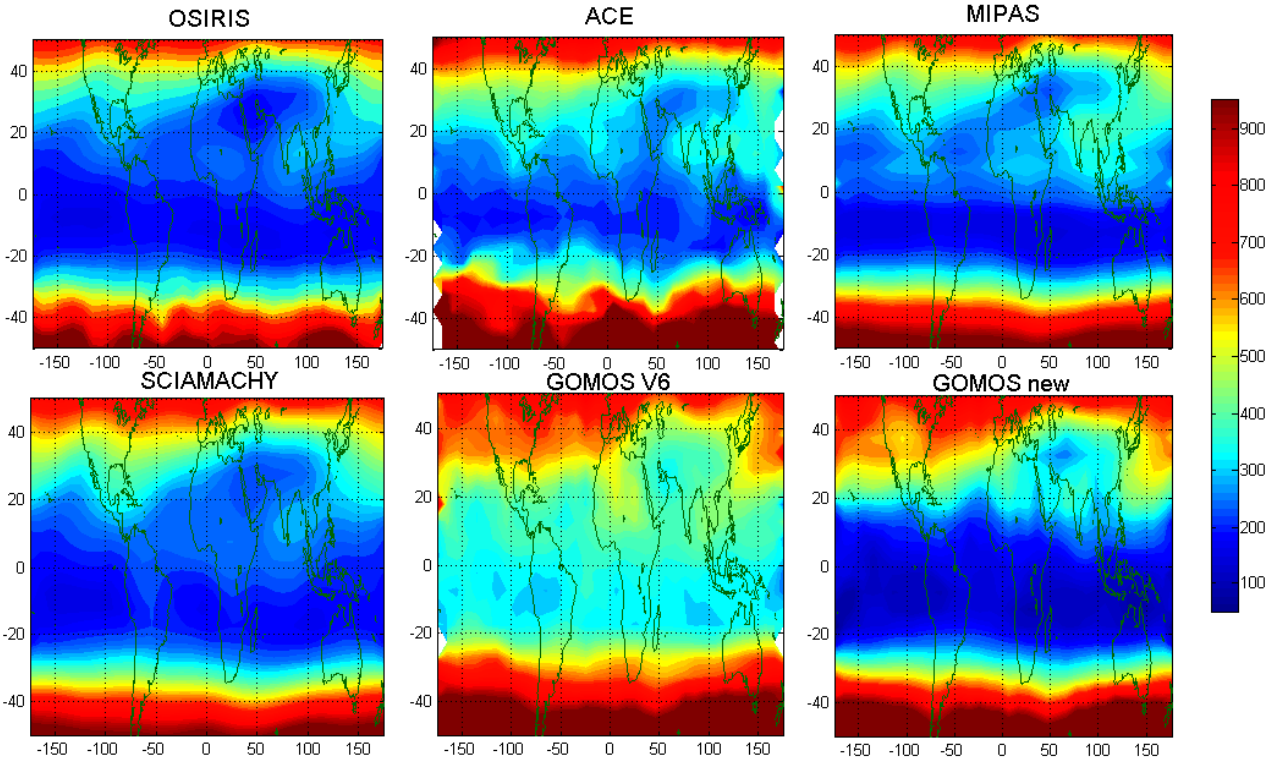

Figure 13. Mean ozone mixing ratio (ppb) at 100 hPa in the summer season (June-August), as inferred from all available measurements by OSIRIS, ACE-FTS, MIPAS, SCIAMACHY and GOMOS (V6 and aerosol-insensitive retrievals).

4 Summary and discussion

The proposed aerosol-insensitive ozone retrieval scheme is very simple. Using relatively narrow wavelength bands allows avoiding the scintillation and dilution correction (allows using Level 1 b transmittances) and reducing uncertainty related to aerosol extinction spectral dependence and removal of Rayleigh scattering. The retrieval algorithm uses minimal assumptions about the

atmospheric profiles. The inversion using visible triplets in the UTLS is stable with respect to variations of reference and absorbing wavelengths.

For the proposed inversion, the ozone profile follow V6 data in the middle atmosphere and follow the triplet ozone profiles in the UTLS and the troposphere. Such an approach seems to be advantageous for the ongoing Ozone_cci project. V6 ozone data have been extensively validated; they exhibit good quality and small biases with respect to ground-based measurements in the stratosphere. The new data will preserve all positive features of V6 in the stratosphere (and makes valid various intercomparison results) and have a significantly improved quality in the UTLS.

Validation of the new retrieved results with ozone sondes and their comparison with V6 data has shown dramatic reduction of ozone biases in the UTLS, especially in the tropics. The validation results with the aerosol-insensitive inversion is very similar to that from the previous processor (GOMLAB) using a linear aerosol extinction model (Sofieva et al., 2015).

Nowadays, the whole GOMOS dataset is processed ("good" stars, sza>107°). The new ozone profiles are in good agreement with ozone sondes and other satellite data having a good quality in the UTLS. The geophysical phenomena are seen by the GOMOS dataset, but the coverage of the UTLS data by GOMOS is limited.

The new ozone dataset will be delivered in the user-friendly Ozone_cci netcdf format [*Sofieva et al.*, 2013], on both pressure and altitude grid. It is expected that it will replace the current GOMOS dataset used in the Ozone_cci project.

5 References

Flittner, D. E., P. K. Bhartia, and B. M. Herman (2000), O3 profiles retrieved from limb scatter measurements: Theory, *Geophys. Res. Lett.*, *27*(17), 2601–2604, doi:10.1029/1999GL011343. [online] Available from: http://dx.doi.org/10.1029/1999GL011343

Kunze, M., P. Braesicke, U. Langematz, G. Stiller, S. Bekki, C. Brühl, M. Chipperfield, M. Dameris, R. Garcia, and M. Giorgetta (2010), Influences of the Indian Summer Monsoon on Water Vapor and Ozone Concentrations in the UTLS as Simulated by Chemistry–Climate Models, *J. Clim.*, *23*(13), 3525–3544, doi:10.1175/2010JCLI3280.1. [online] Available from: http://dx.doi.org/10.1175/2010JCLI3280.1

Park, M., W. J. Randel, A. Gettelman, S. T. Massie, and J. H. Jiang (2007), Transport above the Asian summer monsoon anticyclone inferred from Aura Microwave Limb Sounder tracers, *J. Geophys. Res. Atmos.*, *112*(D16), D16309, doi:10.1029/2006JD008294. [online] Available from: http://dx.doi.org/10.1029/2006JD008294

Sofieva, V. F. et al. (2013), Harmonized dataset of ozone profiles from satellite limb and occultation measurements, *Earth Syst. Sci. Data*, *5*(2), 349–363, doi:10.5194/essd-5-349-2013. [online] Available from: http://www.earth-syst-sci-data.net/5/349/2013/

Sofieva, V., E. Kyrölä, I. Ialongo, J. Hakkarainen and J. Tamminen: Improved GOMOS two-step inversion algorithm in the Upper Troposphere and Lower Stratosphere, Technical Note, 2015.